Received: 17 October 2022 | Revised: 24 November 2022 | Accepted: 12 December 2022

DOI: 10.1002/nano.202200223

RESEARCH ARTICLE

nano select Open Access WILEY

Synthesis and properties of COK-12 large-pore mesocellular silica foam

Laura M. Henning[1] | **Glen J. Smales**[2] | **Maria Gracia Colmenares**[3] | **Maged F. Bekheet**[1] | **Ulla Simon**[1] | **Aleksander Gurlo**[1]

[1]Technische Universität Berlin, Faculty III Process Sciences, Institute of Material Science and Technology, Chair of Advanced Ceramic Materials, Berlin, Germany

[2]Division 6.5 – Polymers in Life Sciences and Nanotechnology, Bundesanstalt für Materialforschung und -prüfung (BAM), Berlin, Germany

[3]GaeaStar GmbH, Berlin, Germany

Correspondence
Laura M. Henning, Technische Universität Berlin, Faculty III Process Sciences, Institute of Material Science and Technology, Chair of Advanced Ceramic Materials, Straße des 17. Juni 135, 10623 Berlin, Germany.
Email: laura.m.henning@ceramics.tu-berlin.de

Abstract

Large, ink-bottle-shaped pores in mesocellular foams (MCFs) are desired for various applications requiring enhanced mass transfer or the immobilization of larger compounds. Hence, the cylindrical pores of COK-12, an ordered mesoporous silica structurally comparable to SBA-15 but synthesized at room-temperature at quasi-neutral pH, are chemically swollen into ink-bottle pores. Therefore, *p*-xylene is used as a more sustainable swelling agent compared to popular alternatives. Its high boiling point allows for an additional thermal aging step to amplify the mesostructure enlargement without needing additional chemicals. For COK-12, the MCFs obtained at room temperature reach an unprecedented plateau for the modal mesopore cell and window diameter of 19.9 and 5.5 nm, respectively, with an underlying broad pore size distribution and distorted hexagonal lattice up to 14.5 nm, involving hexagonal and spherical structures. The combined chemical and thermal swelling resulted in the selective enlargement of the window diameter to more than 200% and a slightly increased cell diameter, pore size distribution, and hexagonal lattice distortion in comparison to the room temperature synthesis. Such materials are thought to be promising alternatives to SBA-15-based MCFs, often utilizing toxic catalysts during synthesis. The presented results pave the way for enhanced adsorptive, catalytic, and drug delivery performances for COK-12-based materials.

KEYWORDS
COK-12, ink-bottle pores, mesocellular foam, ordered mesoporous silica

1 | INTRODUCTION

Ordered mesoporous silicas (OMSs) are materials with highly ordered mesopores, high specific surface areas (SSAs), and high pore volumes. Their properties make them interesting for a wide range of applications, such as catalysis, water and air treatment, sensor engineering, and drug delivery.[1–5] While MCM-41 and SBA-15 remain the most prevalent OMSs, COK-12 has appeared as a promising alternative to SBA-15 materials owing to its more environmentally friendly room-temperature synthesis at quasi-neutral pH, its scalability, and its use of an inexpensive silica source.[6–8] COK-12's representative static aging at room temperature, requiring no energy input,

and advancements in the reduction of the calcination time facilitate low energy requirements.[7,9,10] Furthermore, the synthesis buffered at mild pH and at ambient temperature and pressure can be considered to be safer than handling strongly acid solutions during hydrothermal synthesis routes, as required for SBA-15.[11] Finally, due to the overall ease of the COK-12 synthesis, successes toward upscaled and continuous procedures have been reported.[7,9,12]

In general, by using a surfactant-templated synthesis route, the OMS mesostructure (e.g., hexagonal, lamellar, cubic, disordered), morphology (e.g., spheres, rods, crystals), and size (in the micro-, meso, and/or macropore range) can be tailored by controlling the synthesis conditions such as surfactant composition and concentration, temperature, pH, and through the choice of additives.[13] Driven by the vast development potential of OMS, siliceous mesocellular foams (MCFs) were first reported on in 1999.[14] MCFs are generally comprised of 3D interconnected spherical cells connected by narrower windows, also referred to as ink-bottle pores.[14,15] Their large-pore structures allow for enhanced mass transfer and the convenient immobilization of bulky functional groups or molecules, paving the way for the adsorption, conversion, or the controlled release of larger molecules.[16–18]

In surfactant-templated syntheses, MCFs can be obtained by the incorporation of a sufficient amount of swelling agent, which accumulates in the micelle center and results in a pore growth and transformation of the initial shape (e.g., hexagonal to the MCF structure).[19] For amphiphilic surfactant molecules made from poly(ethylene oxide)-poly(propylene oxide)-poly(ethylene oxide) (PEO-PPO-PEO) block copolymers, for example, Pluronic P123, which is utilized in the synthesis of the OMS materials SBA-15 and COK-12,[6,11] swelling agents with a hydrophobic character are applied, accumulating within the hydrophobic PPO core of the micelle. For P123-based ($EO_{20}PO_{70}EO_{20}$) MCFs of the SBA-15 type, aromatic compounds, such as 1,3,5-trimethylbenzene (TMB) and xylene, yet only in combination with aqueous ammonia, have been reported as swelling agents and are most commonly used at concentrations of 0.5–2 grams per gram of P123, with TMB being utilized significantly more often.[14,19–23] Furthermore, hexane has been successfully utilized as a swelling agent to obtain MCFs from both SBA-15 and COK-12 type materials.[8,15,24] Additionally, TMB was used to demonstrate the flexibility of the micelles in the COK-12 synthesis by small-angle X-ray scattering (SAXS) measurements, yet the final structure upon template removal was not fully characterized.[7]

To further tailor the mesostructure of MCFs in the presence of swelling agents, different pathways are available. Firstly, NH_4F is commonly applied as a catalyst and mineralizing agent to selectively enlarge the window size by up to 80%.[14,25–27] Thereby, fluorides such as NH_4F increase the solubility of silica in water, allowing to reverse the hydrolysis and condensation and thus, improve the structural organization of the silica.[25,28] Secondly, temperature, pH adaptors such as aqueous ammonia or hydrochloric acid, and their time of incorporation can be used to affect the hydrolysis rate and extent of template self-assembly to further enlarge the pore cell size.[22,29] Lastly, a prolonged aging time was found to broaden the overall pore size distribution, including larger pores.[29,30]

While F127-based ($EO_{102\text{-}106}PO_{70}EO_{102\text{-}106}$) face-centered OMS materials such as FDU-12 or COK-19 directly yield spherical mesopores, which can be expanded with swelling agents such as TMB, ethylbenzene, or xylene,[31–33] their suitability for the synthesis of MCFs is generally limited due to the longer EO blocks and about two times higher block copolymer costs, restricting desired generous cell interconnectivity and cost efficiency, respectively. However, temperature elevation throughout the synthesis was shown to enhance the mesopore interconnectivity of the face-centered OMS materials FDU-12 and COK-19, with and without the use of swelling agents, respectively.[31,33]

The aim of this work is to study the suitability and efficiency of *p*-xylene as a swelling agent for the hexagonal OMS COK-12 toward obtaining large-pore MCFs and thoroughly examine the resulting structural properties. Thereby, *p*-xylene is chosen over TMB and hexane because it is more cost-effective and its boiling point (138.4°C) is higher than that of hexane (69°C), allowing for an additional thermal aging step at 90°C. Furthermore, in contrast to TMB and hexane, *p*-xylene does not constitute an acute or chronic environmental hazard according to the Globally Harmonized System of Classification and Labelling of Chemicals 09 (GHS09). The additional thermal aging step at 90°C in the presence of only a small amount of swelling agent allows to further enlarge the mesostructure and converge pore cell and window sizes, pursuing a greener alternative in contrast to the extensive use of chemicals such as swelling agents or catalysts.

2 | EXPERIMENTAL

2.1 | Chemicals

Pluronic P123 (MW ~ 5800 g mol^{-1}) and *p*-xylene (99%, density of 0.861 g cm^{-3} at 20°C) were purchased from Sigma-Aldrich (Merck, Germany). Citric acid (≥99.5%, anhydrous), trisodium citrate dihydrate (≥99%), and sodium silicate (7.8–8.5 wt% Na_2O, 25.8–28.5 wt% SiO_2)

were obtained from Carl Roth (Germany). Deionized water (DIW) was used for the synthesis and washing.

2.2 | COK-12 synthesis

COK-12 was synthesized as reported previously, including the incorporation of a swelling agent.[15,34] Instead of n-hexane, *p*-xylene was utilized as a swelling agent. Briefly, 4 g P123 was dissolved in 107.5 mL DIW. Upon dissolution of P123, different volumes of *p*-xylene, that is, 0, 0.25, 0.5, 0.75, 1, 2, and 4 mL per gram of P123, were incorporated and stirring was continued overnight. After 13 hours, 3.362 g anhydrous citric acid and 2.882 g trisodium citrate dihydrate were added as a buffer. After another 7 hours, a mixture of 10.4 g sodium silicate and 30 mL DIW was added and stirring was maintained for 5 minutes. Thereafter, the slurry was aged at room temperature for 24 hours without stirring and then gradually washed with 500 mL DIW. Finally, the material was dried at 60°C overnight and calcined in air at 500°C with a 1 K min^{-1} heating rate and 8 hours dwell time to remove the templating agent. The resulting materials were denoted COK-12-X#, where # represents the volume of *p*-xylene in mL incorporated per gram of P123.

A batch upscaled by a factor of five was produced using 0.5 mL *p*-xylene per gram of P123 and applying an additional aging step at elevated temperature, during which the slurry was kept at 90°C for 24 hours, in a closed system to avoid solvent evaporation, following the aging at room temperature and prior to the washing step, as previously investigated.[6,10] The aging temperature of 90°C was chosen to maximize the thermal swelling effect, while preventing possible structure-alterations from the boiling of aqueous system. The resulting material was denoted COK-12-X0.5+A.

2.3 | Characterization

The pore structure, pore size, and SSA were studied using nitrogen sorption analysis in a QuadraSorb apparatus (Quantachrome, USA). Isotherms were recorded at 77 K after degassing under vacuum for 10 hours at 200°C. The SSA was determined using the Brunauer, Emmet and Teller (BET) method. Model applicability was ensured using the Rouquerol plot.[35,36] The mesopore cell and window diameters were determined from the nonlocal density function theory (NLDFT) calculations on the adsorption and desorption branches of the isotherm, respectively. The cylindrical/spherical pore model, valid for cylindrical pores with pore diameters smaller than 5 nm and spherical pores larger than 5 nm,[37] was used on the adsorption branch to account for the dominant, ink-bottle structure for samples with high *p*-xylene volumes ($X \geq 0.75$). For low amounts of *p*-xylene ($X \leq 0.5$), the dominant cylindrical mesopore structure was obtained using the cylindrical pore model applicable to all mesopore sizes. The cylindrical pore model was also applied to the desorption branch to determine the window sizes. Micropores were analyzed by the t-plot method.[38] All nitrogen sorption data was analyzed using the Quantachrome ASiQwin software (Version 4.01).

SAXS data was collected using the MOUSE instrument at the Bundesanstalt für Materialforschung und -prüfung (BAM).[39] A monochromatized Cu Kα (λ = 0.154 nm) X-ray source was used and data were collected using an in-vacuum Eiger 1 M detector (Dectris, Switzerland), which was placed at multiple distances between 57 and 2507 mm from the sample. Powder samples were sandwiched between two pieces of Scotch Magic™ tape. Data was subsequently processed using the DAWN software package using standardized data correction procedures.[40,41] Fitting of the SAXS data was performed using a previously reported SAXS fitting model with some additions to better describe the swollen and ink-bottle shaped pores.[12] In short, fitting of the SAXS data was performed using SASfit,[42] allowing for information on the lattice parameter, macro-/ meso-/ and micropore sizes, alongside an additional spherical contribution, and in some cases, a second hexagonal contribution, to account for the spherical cells with ink-bottle shaped pores and enlarged window sizes of the thermally swollen COK-12-X0.5+A. More detailed information on the SAXS modelling can be found in the SI (Figures S1–S3).

Particle morphology was investigated by means of scanning electron microscopy (SEM) using a LEO Gemini 1530 (Zeiss, Germany) at 5 kV with an InLens electron detector and an aperture size of 30 μm after sputtering with a thin carbon layer.

The mesostructure was visualized with a transmission electron microscope (TEM) in a FEI Tecnai G^2 20 S-TWIN (FEI, USA) equipped with a LaB_6-source at 200 keV acceleration voltage. Images were recorded with a GATAN MS794 P CCD-camera.

3 | RESULTS AND DISCUSSION

The nitrogen sorption analysis results, depicted in Figure 1a, show that the pristine COK-12-X0 possesses a typical type IVa isotherm with a H1 hysteresis loop, characteristic for the cylindrical mesopores with a narrow pore size distribution and in agreement with previous works.[6,7,9,10,36,43,44] Upon the addition of *p*-xylene, the main hysteresis loop is shifted toward higher relative

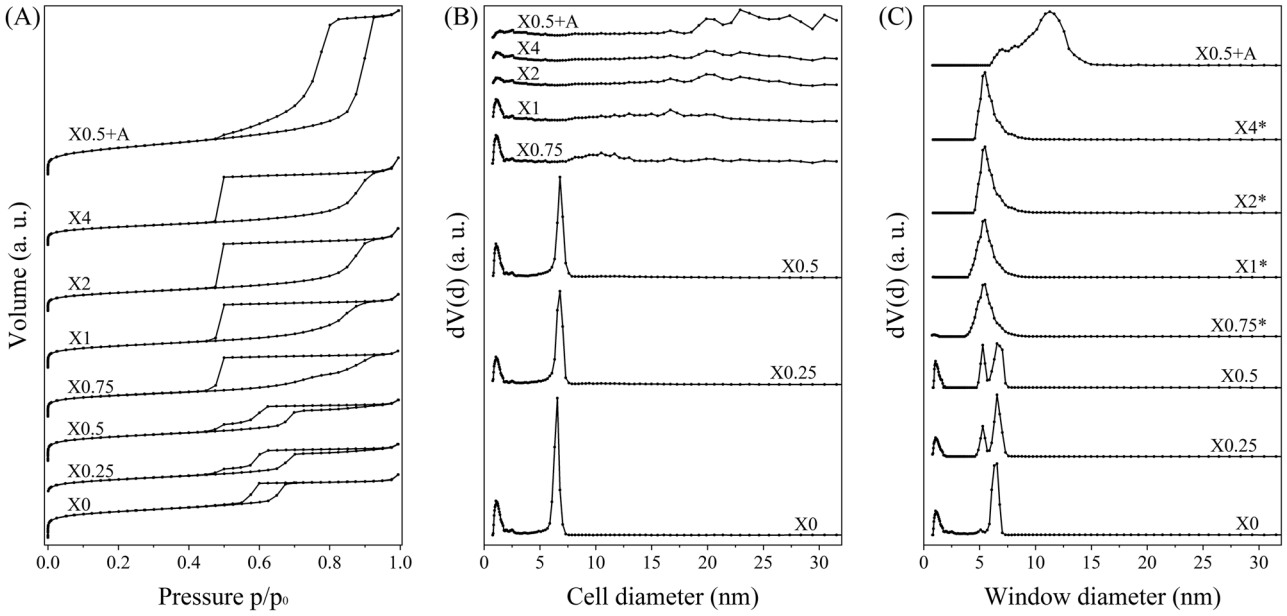

FIGURE 1 a) Nitrogen sorption isotherms, b) the corresponding cell-, and c) window pore size distributions obtained by NLDFT from the adsorption and desorption branch of COK-12-X# synthesized with 0–4 mL swelling agent *p*-xylene per gram of P123 (X0–X4). The +A represents an additional thermal aging step at 90°C. All graphs are stacked by 10% (absolute) for clarity. The original isotherms are shown in Figure S4. The graphs marked with an asterisk (*) are to be treated with care due to fitting errors of up to 8%, compare Figure S5.

pressures while the hysteresis onset is shifted toward lower relative pressures, indicating an increase in the main mesopores size as well as a boosted presence of smaller mesopores, compare also the original isotherms displayed in Figure S4. When an additional aging step at 90°C is induced for COK-12-X0.5+A, the onset position of the hysteresis loop remains constant, yet its width and height are markedly enlarged toward higher pressures and volumes, indicating a broader pore size distribution, increased SSA, larger mesopores, and higher pore volume. For COK-12 samples synthesized with higher volumes of *p*-xylene (X ≥ 0.75), a H2a hysteresis loop can be observed, which is characteristic for the ink-bottle pores of MCFs, where desorption is decoupled from the cell pore size and dependent on the smaller window size minimizing the entrance, delaying capillary evaporation.[15,36,45] The development of the cell and window diameters obtained from the application of NLDFT models on the adsorption and desorption branches, respectively, is depicted in Figure 1b,c. A summary of all obtained parameters is also listed in Table 1. Starting off with cylindrical mesopores of 6.6 nm in diameter, a BET SSA of 634 $m^2\ g^{-1}$, pore volume of 0.61 $cm^3\ g^{-1}$, and a micropore volume of 0.13 $cm^3\ g^{-1}$ for the pristine COK-12-X0, an increase in the cell diameter along with a slight decrease in window diameter, (micro-) pore volume, and SSA can be observed upon the addition of *p*-xylene. For COK-12-X0.25 and COK-12-X0.5, a transition phase occurs, which is characterized by a bimodal mesopore diameter distribution, where the second peak corresponds to the window sizes shifting toward smaller diameters. Finally, the cell diameter and pore volume reach a plateau at 19.9 nm and 0.73 $cm^3\ g^{-1}$, respectively, for COK-12-X2 and COK-12-X4. Concurrently, the mesopore size distributions are significantly broadened, as previously derived from the hysteresis shapes of the isotherm, limiting the significance of the common modal pore size. Furthermore, the window diameter, micropore volume, and consequently also the SSA of the series settle at 5.5 nm, 0.07 $cm^3\ g^{-1}$, and 434 $m^2\ g^{-1}$, respectively, at the plateau of COK-12-X2 and COK-12-X4. It must be noted that for these predominantly MCF-based structures with large cell sizes, the applicability of the cylindrical NLDFT model on the desorption branch is restricted, as shown in Figure S5, yielding fitting errors up to 8%, wherefore the window sizes for these samples must be treated with care. The observed change from cylindrical mesopores toward MCFs with ink-bottle pores is reported to be driven by the reduction of the surface to volume ratio to cover an increasing amount of hydrophobic swelling agent with the same amount of templating agent P123 and is described as buckling of the cylindrical pores with approximately the same periodicity as the pore diameter, forming spherical nodes along the pore length.[19] The observed decrease in microporosity, which is located in the silica walls between the pores and noticeably constitutes to the total SSA, can be expected to arise from the reduced wall thickness caused by the pore buckling, as previously observed.[30]

TABLE 1 Structural parameter summary for COK-12-X# synthesized with 0–4 mL swelling agent *p*-xylene per gram of P123 (X0–X4)

Sample COK-12-	$D_{c,N2}$[a] [nm]	$D_{w,N2}$[b] [nm]	S_{BET}[c] [$m^2\ g^{-1}$]	V_{N2}[d] [$cm^3\ g^{-1}$]	$V_{micro,N2}$[e] [$cm^3\ g^{-1}$]	a[f] [nm]	a distortion[g] [%]	$D_{micro,S}$[h] [nm]	$D_{c,S}$[i] [nm]	$D_{w,S}$[j] [nm]	$D_{macro,S}$[k] [nm]
X0	6.6[l]	6.6	634	0.61	0.13	10.6	<1	0.89	-	6.4	169
X0.25	6.8[l]	6.6	537	0.56	0.11	11.0	<1	1.01	7.6	7.2	170
X0.5	6.8[l]	6.6	587	0.59	0.13	11.0	<1	1.04	7.6	7.4	173
X0.75	10.5[m]	5.5[n]	510	0.61	0.11	11.7	6.6	1.17	15.5	5.4	193
X1	16.7[m]	5.5[n]	522	0.67	0.10	12.0	6.7	1.18	16.3	5.4	196
X2	19.9[m]	5.5[n]	434	0.72	0.07	13.9	9.7	1.71	18.7	5.4	199
X4	19.9[m]	5.5[n]	434	0.73	0.07	14.5	9.7	1.74	19.2	5.4	200
X0.5+A	22.9[m]	11.3	640	1.55	0.07	15.2/10[o]	2.2/ 3.7[o]	1.87	22.4	6.5/5.6[o]	200

[a]Mesopore cell diameter estimated by NLDFT on N_2-adsorption branch.
[b]Mesopore window diameter estimated by NLDFT on N_2- desorption branch
[c]Specific surface area (SSA) estimated by the BET method
[d]Pore volume estimated by NLDFT on N_2-adsorption branch
[e]Micropore volume estimated by the t-plot method
[f]Lattice parameter determined by SAXS
[g]Distortion of the hexagonal lattice position determined by SAXS
[h]Micropore diameter determined by SAXS
[i]Mesopore cell diameter determined by SAXS (spherical contribution)
[j]Mesopore window diameter parameter determined by SAXS (hexagonal contribution)
[k]Macropore diameter determined by SAXS
[l]NLDFT cylindrical pore model
[m]NLDFT cylindrical/spherical pore model
[n]Data to be treated with care due to fitting error of up to 8%
[o]Obtained from two hexagonal contributions.
The +A represents an additional thermal aging step at 90°C.

Upon the application of an additional aging step at 90°C for COK-12-X0.5+A, the cell diameter distribution is further broadened and shifted toward larger mesopores of about 18.5 nm up to more than 30 nm with a mode pore diameter of 22.9 nm. Similarly, the additional aging step at 90°C also broadens the window diameter distribution and shifts the modal window size to 11.3 nm. The pore size broadening is likely to be attributed to both the elevated temperature and prolonged aging time, affecting the silica dissolution and reprecipitation.[10,29,30] Furthermore, the upscaling of the synthesis by a factor of five might have slightly contributed to broadening of the pore diameter toward larger values as indicated from COK-12 pore sizes obtained from batches upscaled by the factors 25 and 50, respectively.[9,12] In accordance with the larger mesopores of COK-12-X0.5+A, the pore volume and SSA increase up to 640 $m^2\ g^{-1}$ and 1.55 $cm^3\ g^{-1}$, while the micropore volume remains at about 50% of the micropore volume of COK-12-X0 and COK-12-X0.5. The enhanced pore swelling and loss of microporosity due to aging at 90°C, despite the smaller *p*-xylene concentration, can be ascribed to two phenomena: On the one hand, the *p*-xylene undergoes thermal expansion with increasing temperature. As its density decreases from 0.861 g cm^{-3} at 20°C to 0.800 g cm^{-3} at 90°C,[46] its volume increases accordingly. On the other hand, the lengths of the ethylene oxide segments of the P123, around which the silica walls are formed, decrease with increasing temperature due to a rapidly increased probability for non-polar anti conformation at elevated temperatures, that is, more hydrophobic behavior, in contrast to the preferred gauche and trans conformation around the C–C bond and C–O bond, respectively, at room temperature, coming along with a large dipole moment.[47,48] This results in a redistribution of the ethylene oxide segments from the silica framework to the region adjacent to the micelle core, expanding the majority of micropores into the mesotunnels and increasing the mesopore size.[20] Accordingly, thermal aging of COK-12 without the utilization of additional swelling agents was previously found to linearly increase the pore size with increasing aging temperature up to 8.1 and 9.4 nm at 90°C, as determined by NLDFT and BJH, respectively, without changing the hexagonally ordered, cylindrical mesopore structure.[6,10] The additional presence of a swelling agent enhances the described phenomenon, yielding extraordinarily large mesopores, with a broad distribution and ink-bottle morphology. The broader mesopore size distribution might furthermore be related to the enhanced solubility of *p*-xylene in water at elevated temperatures,[49] likely causing it to advance into the hydrophilic PEO moieties.

The increase in pore diameter and change in pore morphology of COK-12 with increasing *p*-xylene

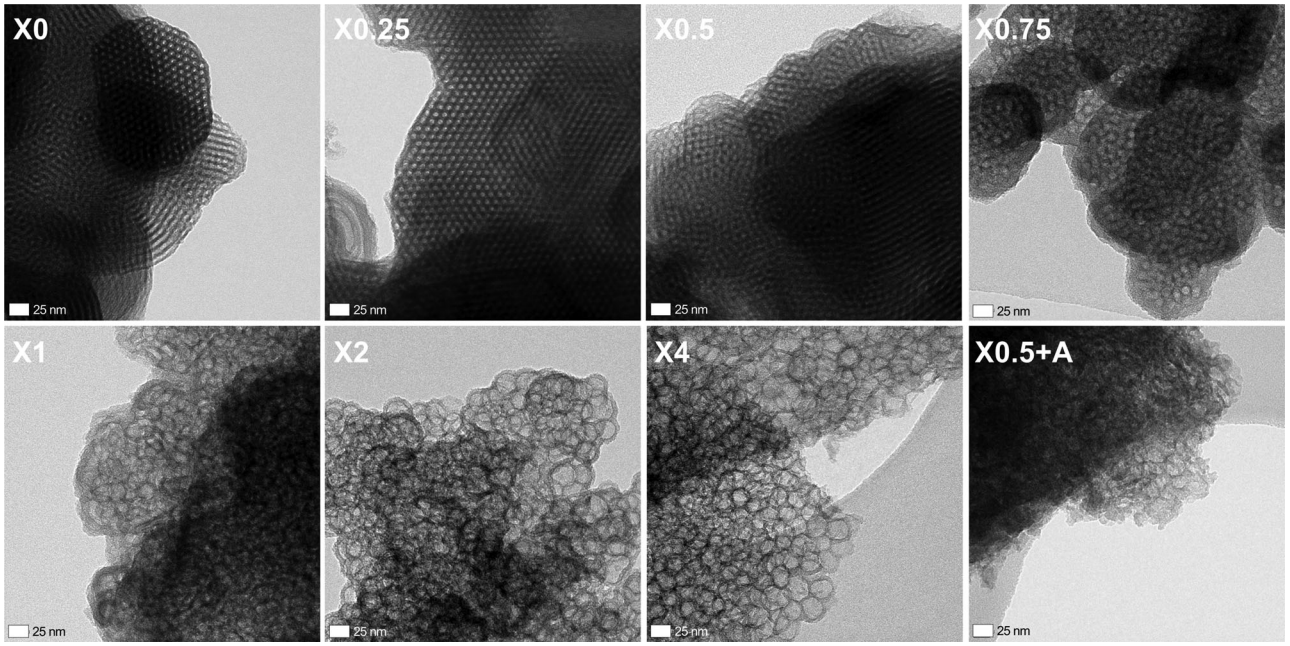

FIGURE 2 TEM images of COK-12-X# synthesized with 0–4 mL swelling agent *p*-xylene per gram of P123 (X0–X4) showing the transformation of the hexagonal ordering of the mesopores into a mesocellular foam. The +A represents an additional aging step at 90°C, inducing further mesopore growth. Scale bars are 25 nm.

concentration, as previously observed by the nitrogen sorption measurements, is revealed by TEM depicted in Figure 2. While the hexagonally ordered mesostructure is maintained for the samples synthesized with low volumes of *p*-xylene (X = 0–0.5), it is much more distorted at higher volumes (X ≥ 0.75), and superseded by the MCF structure. The transition is reflected by vaguely perceivable curved cylindrical pores, something that is reported to be an intermediate structure in the transfer from hexagonal cylindrical pores to MCF.[23] While the mesopores appear mostly uniform in size with clean edges up to COK-12-X4, the pore sizes become much less uniform for COK-12-X0.5+A. Furthermore, the pore walls of COK-12-X0.5+A are only faintly visible and seem frayed at the particle edges. Overall, the majority of the mesopores in Figure 2, in particular for COK-12-X2 and higher, appear to be ca. 20 nm in diameter in accordance with the pore size distribution of the nitrogen sorption data.

The SAXS patterns and corresponding fits of the COK-12 powders are shown in Figure 3, allowing for the evaluation of the influence of the swelling agent on the hexagonal lattice and pore structures. For the COK-12 samples obtained using low volumes of *p*-xylene (X = 0–0.5), at least three well-resolved reflections can be observed clearly at distances corresponding to $q_1:q_2:q_3 = 1:\sqrt{3}:\sqrt{4}$, indexed as (10), (11), and (20), satisfying the conditions for the 2D hexagonal symmetry *P6m* observed in the TEM images in Figure 2. In comparison to the pristine COK-12-X0 with a lattice parameter of 10.6 nm, the reflections of the

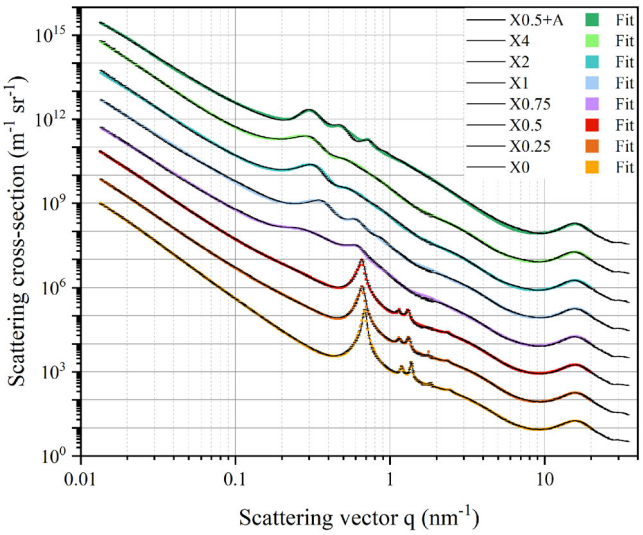

FIGURE 3 SAXS patterns and corresponding fits for COK-12-X# synthesized with 0–4 mL swelling agent *p*-xylene per gram of P123 (X0–X4), vertically shifted for clarity. The +A represents an additional thermal aging step at 90°C.

SAXS patterns are shifted toward a lower scattering vector for COK-12-X0.25 and COK-12-X0.5, indicating a slight increase in d-spacing and accordingly, an increase in the lattice parameter to 11.0 nm for low concentrations, as visualized in Figure 4. It is also notable that the hexagonal lattices are relatively unaffected, as seen from the low distortion values <1% in Table 1. However, for the COK-12

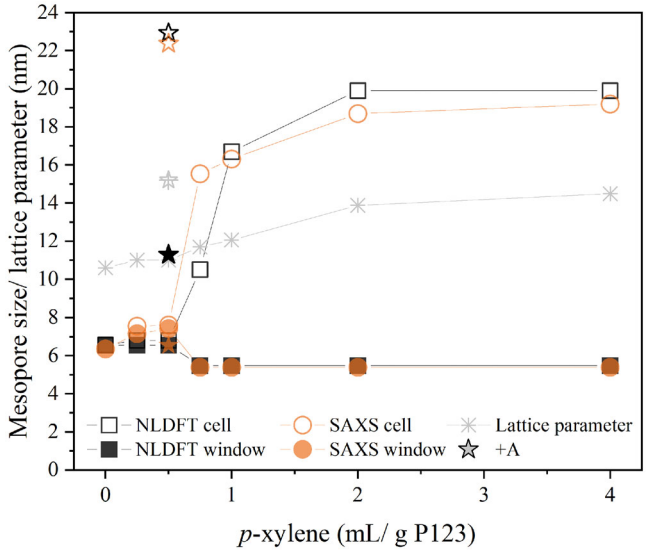

FIGURE 4 Lattice parameter and cell and window sizes of the mesopores for COK-12-X# synthesized with 0–4 mL swelling agent *p*-xylene per gram of P123 (X0–X4) as determined by nitrogen sorption (grey) and SAXS fitting (orange). The stars represent the respective values for COK-12-X0.5+A, synthesized with an additional thermal aging step at 90°C. The full size distributions can be found in Figures 1 and S6.

samples obtained with higher volumes of *p*-xylene ($X \geq 0.75$), the reflections corresponding to the hexagonal lattice attenuate considerably, while further shifting toward lower scattering vectors and thus, larger lattice parameters up to a maximum lattice parameter of 14.5 nm for COK-12-X4, compare Figure 4 and Table 1. Superseded by a hard sphere contribution, not conforming to any other plane or space group such as the cubic symmetry, the hexagonal lattice is significantly distorted as a result of the previously described buckling upon the addition of *p*-xylene, resulting in distortions up to 9.7%. Finally, the implementation of an additional aging step at 90°C for the COK-12-X0.5+A sample results in the necessity for a second hexagonal contribution in the SAXS model to obtain a reasonable fit, see Figure S3. In comparison to the sample COK-12-X0.5, which was swollen at room temperature, the distortions of the hexagonal lattices are higher for the thermally aged sample with the same *p*-xylene concentration COK-12-X0.5+A. The overlap of the mesopores with two distorted hexagonal lattices results in the appearance of an irregular and disrupted mesopore structure, as previously observed from the TEM images in Figure 2.

In addition to the size and distortion of the lattice parameter, the SAXS model allows to obtain data on the micro-, meso-, and macropores of the COK-12-X# powders, listed in Table 1, together with the mesopore data obtained from the nitrogen sorption analysis. Firstly, an increase in the micropore size from originally about 1 nm for COK-12-X0 to 1.74 nm for COK-12-X4 can be observed from the SAXS data with increasing *p*-xylene content. Hence, the corresponding volume-weighted microsize distributions broaden and the relative micropore volumes decrease with increasing amount of *p*-xylene, in particular for COK-12-X2 and COK-12-X4, as shown in Figure S6. This finding is in accordance with the results obtained on the micropore development using the nitrogen sorption analyses, yet with a higher resolution and shorter measurement time. While the nitrogen sorption measurements, including the low-pressure data points for the determination of the micropore data, require about 28–57 hours per sample for the presented datasets, all samples could be loaded into a SAXS multi-sample holder at once, corresponding to a measurement time per sample of ca. 8.5 hours, including measurement overlaps, allowing to additionally monitor the sample stability in vacuum, which might be of greater interest for non-silica samples.

Secondly, the mesopore window sizes obtained by the SAXS fitting range from 5.4 to 7.4 nm and are in accordance with the data obtained from the nitrogen sorption measurements for the room temperature *p*-xylene series, as depicted in Figure 3, indicating that a fitting error of up to 8% as obtained from the application of the cylindrical NLDFT model might still provide acceptable results for the MCF structures at hand. The slight deviation at low *p*-xylene concentrations is likely to be attributed to the lower sensitivity of the NLDFT method in comparison to SAXS, as previously reported.[12] For COK-12-X0.5+A, the deviation of the SAXS window sizes toward the ones obtained by NLDFT is substantial with differences up to 5.7 nm, which might likely be attributed to the disruption of the remaining hexagonal pore structure, hampering the fitting process of NLDFT, employing highly ordered structures, and possibly also to a small fraction of inaccessible pores. Besides the change in the mesopore window sizes, a decrease in the intensity of the volume-weighted distribution of the mesopore windows can be observed from the SAXS data with increasing *p*-xylene content and temperature, see Figure S6, along with a broadening of the distribution, similar to the observed micropore development. The broader distribution presumably correlates to the bimodal distribution observed in the nitrogen sorption data displayed in Figure 1, yet could not be deconvoluted due to the underlying Log-normal model used in the SAXS fitting, as well as increasing irregularity with increasing *p*-xylene content and elevated temperature. At the same time, as a result of the buckling-induced volume shift from the hexagonal to the spherical contribution, a significant increase in the mesopore cell size and volume can be observed in Table 1 and Figure S6, representing the volume shift into the spherical mesopores.

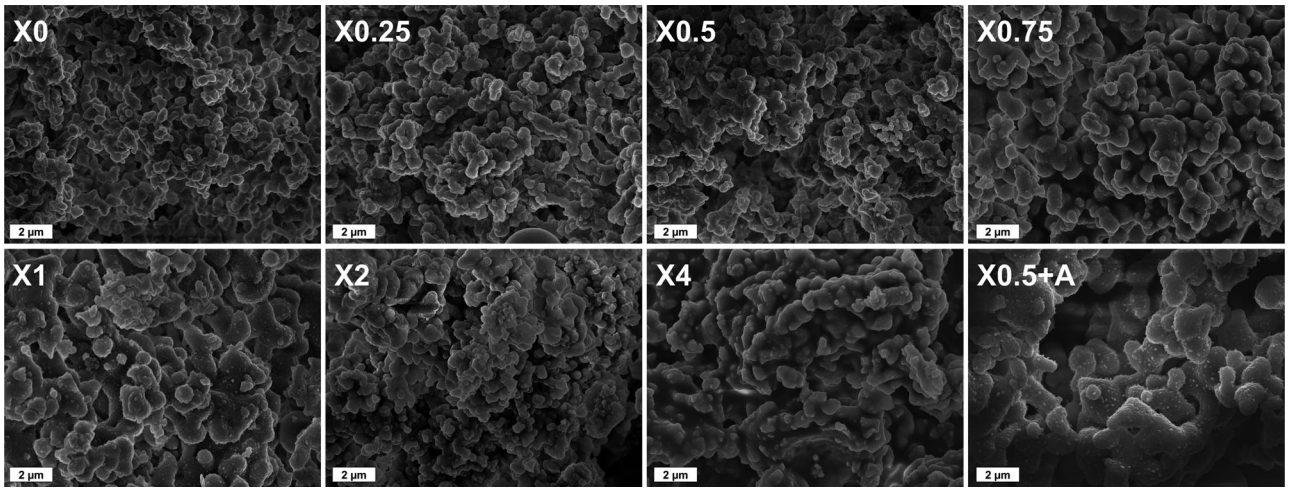

FIGURE 5 SEM images of COK-12-X# synthesized with 0–4 mL swelling agent *p*-xylene per gram of P123 (X0–X4) showing particle growth by aggregation. The A represents an additional thermal aging step at 90°C.

Finally, the SAXS model allows for the evaluation of the macropores of the selected samples. As no structural macroporosity is expected within the powder, unlike those previously observed for COK-12 monoliths,[12] the macropores can be considered to be inter-particle voids. As can be seen from Table 1 and Figure S6, the macropore size gradually increases with increasing *p*-xylene content, which indicates larger voids and accordingly, an increase in the particle size.

SEM micrographs in Figure 5 reveal apparently loosely assembled agglomerates of particles for the pristine COK-12-X0. Upon the addition of *p*-xylene, an increase in the overall particle size can be observed. It is thought that particle aggregation can occur upon the addition of pore expanders, founded on the decreased repulsion between the silica particles due to the higher hydrophobic character of the synthesis medium, in accordance with the presented data.[50] Contrarily, it has been reported that the presence of pore expanders facilitates nucleation and can hinder particle growth, yielding smaller particles.[51] The application of an additional thermal aging step at 90°C for COK-12-X0.5+A yields significantly larger particles in comparison to the merely chemically swelled sample COK-12-X0.5 with overlying smaller particles. The increase in the main particle size can be attributed to increased dehydration of the P123 at higher temperatures, which favors separation from the aqueous solvent environment, leading to higher aggregation numbers.[48] Furthermore, the prolonged aging provides more time for the dissolution of smaller particles and their reprecipitation onto larger particles for COK-12-X0.5+A.[52]

A listing of the maximum structural parameters obtained in this work for COK-12-X# is shown in Table 2, in comparison to other MCFs based on P123, synthesized with various swelling agents, along with their main synthesis parameters. While the comparison of the lattice parameter is strongly limited due to a lack of data, all studies report nitrogen sorption data results for their structures. However, it is worth mentioning that the comparison of the data has to be performed with care. This is due to the fact that there exist difficulties in the unambiguous determination of the BET SSA[53] as well as the non-uniform application of different models to obtain pore sizes and pore volumes, such as the Broekhoff-de Boer (Bdb) model and related methods, Barrett-Joyner-Halenda (BJH) model, and the most recent non-local density function theory (NLDFT) method. While the NLDFT and BdB-related methods are known to be reliable for the structures at hand,[54,55] the BJH method is known to underestimate mesopore sizes.[56,57] From Table 2 it can be seen that the vast majority of MCFs were synthesized based on the recipe of SBA-15 with various concentrations of TMB as a swelling agent and at temperatures above 100°C, yielding a broad range of maximum mesopore cell diameters with significantly smaller mesopore window sizes and partially considerably degraded SSAs. With the objective to enhance the mesopore window sizes, NH_4F was additionally incorporated in a variety of studies, enlarging the pores and diminishing the difference between mesopore cell and window size, which is suitable for enhanced mass transport. Thereby, arrays of spheres were also found to develop into strut-like networks.[14] Other than TMB, hexane, and xylene were deployed for the synthesis of MCFs. It was reported and can be seen from Table 2 that the pore enlargement is less pronounced for hexane than for TMB at the same molarity, most likely due to reduced solubility in the P123 micelle core, whereas alkanes with shorter chain length exhibited a higher solubilization capacity than alkanes with longer lengths.[20,30,58] In comparison, *p*-xylene can be expected

TABLE 2 Overview on MCFs derived from different P123-based OMS types and their maximum structural parameters

OMS type	Swelling agent	Swelling agent/P123 [g/g]	Additional catalyst	Synthesis temp [°C]	D_c[a] [nm]	D_w[b] [nm]	S_{BET}[c] [$m^2\ g^{-1}$]	V_{N2}[d] [$cm^3\ g^{-1}$]	a[e] [nm]	Refs.
SBA-15	TMB	1.5	no	120	36[h]	11[h]	655	1.7	N/A	[14]
SBA-15	TMB	0.5	no	120	31[h]	8.8[h]	N/A	N/A	24.5	[19]
SBA-15	TMB	2	no	100	17.3[i]	11.6[i]	485	2.10	N/A	[23]
SBA-15	TMB	2	no	140	22.3[i]	12.6[i]	254	1.25	13.0	[20]
SBA-15	TMB	1.75	no	120	38.3[h]	7.9[h]	372	1.82	N/A	[21]
SBA-15	TMB	1.25	NH_4F	140	49.5[h]	26.5[h]	N/A	N/A	N/A	[26]
SBA-15	TMB	1.25	NH_4F	140	41.5[i]	22.7[i]	331	2.38	N/A	[27]
SBA-15	TMB	2.5	NH_4F	100	42.0[h]	19.1[h]	595	2.3	N/A	[25]
SBA-15	TMB	1.5	NH_4F	120	36[i]	18[i]	625	2.4	N/A	[14]
SBA-15	hexane	1.75	no	95	16.4[i]	7.6[i]	529	0.72	N/A	[24]
SBA-15	xylene	0.75	NH_4OH	80	18.6	15.3	291	1.34	N/A	[22]
COK-12	TMB	0.2	no	RT	9.7[g]	N/A	N/A	N/A	N/A	[7]
COK-12	n-hexane	4.6 (5.4[f])	no	RT	8.4[j]	5.3[j]	461	0.63	11.5	[8,15]
COK-12	*p*-xylene	1.7 (2[f])	no	RT	19.9[j]	5.5[j]	434	0.72	13.9	This work
COK-12	*p*-xylene	0.4 (0.5[f])	no	90	22.9[j]	11.3[j]	640	1.55	15.2	This work

Abbreviation: N/A, not available.

[a]Mesopore cell diameter

[b]Mesopore window diameter

[c]Specific surface area (SSA) estimated by BET method

[d]Pore volume

[e]Lattice parameter/unit cell parameter

[f]ml swelling agent/g P123

[g]micelle core radius of core-shell composite with 15% of the nominal silica source, determined from SAXS fitting of uncalcined material

[h]Determined from BdB (Broekhoff-de Boer) or BdB-FHH (Broekhoff-de Boer, Frenkel-Halsey-Hill) method

[i]Determined from BJH (Barrett-Joyner-Halenda) method, known to underestimate the mesopore size[56,57]

[j]Determined from NLDFT (non-local density function theory) method.

to be well incorporated in the hydrophobic P123 micelle core due to its practical insolubility with water.[59] The lower efficiency of hexane as a swelling agent can also be seen from the results of utilizing hexane and *p*-xylene as a swelling agent for COK-12 in Table 2. Compared to hexane, *p*-xylene has a stronger effect on the mesopore size increase, even with lower amounts of swelling agent, making it more efficient. In comparison to SBA-15-based MCFs swollen with TMB, the structural parameters of the COK-12-based MCFs swollen with *p*-xylene reach the same range, yet remain at its lower end. This can be attributed to both the higher synthesis temperature of the SBA-15 based MCFs as well as the additional methyl group of TMB over xylene, whose additional carbon atoms enhance the swelling performance.[32] The additional thermal aging step at 90°C for COK-12-X0.5+A results in an assimilation of the mesopore cell and window size, similar to the utilization of NH_4F, but without the thermal decomposition of NH_4F into highly toxic hydrogen fluoride, making the thermal aging step a promising and more environmentally friendly alternative. Additionally, the aging at elevated temperature significantly increases the mesopore size, SSA, and pore volume for COK-12-X0.5+A, even in comparison to the maximum structural parameters obtainable with the room-temperature series utilizing four to eight times higher amounts of *p*-xylene per gram of P123.

4 | CONCLUSION

COK-12 based MCFs were synthesized using *p*-xylene as a less hazardous and more cost-effective swelling agent that allows for an additional thermal aging step at 90°C to further enlarge the mesostructure without needing additional chemicals.

At room temperature, *p*-xylene was found to be an efficient pore swelling agent for COK-12, eliciting a buckling of the hexagonally ordered, cylindrical mesopores and eventually their transfer into a MCF structure with ink-bottle pores. A plateau and at the same time new maximum of the mesopores for COK-12 type materials was reached with cell and window diameters of 19.9 nm and 5.5 nm, respectively, accompanied by a broadening of the pore size distribution.

The fitting results from the custom SAXS model, expanding the hexagonal lattice with a spherical contribution to account for the ink-bottle pores, were found to be in great accordance with the NLDFT model applied on the nitrogen sorption data, allowing to obtain a multi-scale analysis from one time-efficient measurement technique and monitor the distortion of the hexagonal lattice, presenting a powerful alternative over other, more intricate methods such as positron annihilation.

The combination of only small amounts of the chemical swelling agent *p*-xylene, with an additional thermal swelling at elevated temperature, slightly increased the cell diameters and also selectively enlarged the window diameters to more than 200% in comparison to the *p*-xylene plateau at room temperature, as obtained by NLDFT measurements, with a broadened pore size distribution. The strong distortion of the native hexagonal lattice was observed by SAXS. Although the SAXS fitting result for the window size of the dually swollen sample was less consistent with the NLDFT results, despite the addition of a second hexagonal contribution to the model, the observed, specific enlargement of the window diameter upon chemically and thermally combined swelling enabled a promising alternative toward the toxic catalyst NH_4F, commonly used to selectively enlarge the window diameter, and therewith a more environmentally friendly alternative.

Prospectively, the aging time might be shortened with the objective to reduce the extent of broadening of the pore size distribution as well as to save energy and time. If even larger pores are required, the determination of the pore size plateau for the combined swelling method in the presence of higher *p*-xylene concentrations might also be of interest. Finally, the convenient upscalability of the synthesis procedure provides potential for a future large scale production and thus, a widespread deployment in various fields.

Overall, the COK-12 based MCFs, with enlarged mesopore cell and window sizes, are expected to further broaden the scope of applications for COK-12 type materials over the prevalent SBA-15 type materials, for example, toward higher loading with active sites and enhanced mass transfer capabilities for enhanced adsorptive or catalytic performance as well as drug delivery.

AUTHOR CONTRIBUTIONS

Laura M. Henning: conceptualization, methodology, formal analysis, investigation, data curation, writing – original draft, visualization, project administration; Glen J. Smales: conceptualization, methodology, software, validation, formal analysis, data curation, writing – original draft, visualization; Maria Gracia Colmenares: conceptualization; writing – review & editing; Maged F. Bekheet: conceptualization, methodology, writing – review & editing, supervision; Ulla Simon: conceptualization, methodology, writing – review & editing, supervision; Aleksander Gurlo: conceptualization, resources, writing – review & editing, supervision, funding acquisition.

ACKNOWLEDGMENTS

We would like to thank Christina Eichenauer for nitrogen sorption measurements, Johannes Schmidt for assisting with the nitrogen sorption data analysis, Fabian Zemke for SEM imaging, and Jan R. J. Simke for TEM imaging (ZELMI), all from Technische Universität Berlin.

Open access funding enabled and organized by Projekt DEAL.

CONFLICT OF INTEREST

The authors declare no conflict of interest.

DATA AVAILABILITY STATEMENT

The data that support the findings of this study are available from the corresponding author upon reasonable request.

REFERENCES

1. S. Pulinthanathu Sree, E. Breynaert, C. E. A. Kirschhock, J. A. Martens, *Front. Chem. Eng.* **2022**, *4*, 810443.
2. S. Jafari, H. Derakhshankhah, L. Alaei, A. Fattahi, B. S. Varnamkhasti, A. A. Saboury, *Biomed. Pharmacother.* **2019**, *109*, 1100.
3. B. Singh, J. Na, M. Konarova, T. Wakihara, Y. Yamauchi, C. Salomon, M. B. Gawande, *Bull. Chem. Soc. Jpn.* **2020**, *93*, 1459.
4. T.-L. Chew, A. L. Ahmad, S. Bhatia, *Adv. Colloid Interface Sci.* **2010**, *153*, 43.
5. A. A. Nada, M. F. Bekheet, S. Roualdes, A. Gurlo, A. Ayral, *J. Mol. Liq.* **2019**, *274*, 505.
6. J. Jammaer, A. Aerts, J. D'Haen, J. W. Seo, J. A. Martens, *J. Mater. Chem.* **2009**, *19*, 8290.
7. J. Jammaer, T. S. van Erp, A. Aerts, C. E. A. Kirschhock, J. A. Martens, *J. Am. Chem. Soc.* **2011**, *133*, 13737.
8. M. Colmenares, Ordered Mesoporous silica COK-12: Mesoscale tailoring, upscaling, continuous synthesis and application in the oxidative coupling of methane. Dissertation, Technische Universität Berlin, **2018**.
9. M. G. Colmenares, U. Simon, O. Cruz, A. Thomas, O. Goerke, A. Gurlo, *Microporous Mesoporous Mater.* **2018**, *256*, 102.
10. L. M. Henning, D. D. Cubas, M. G. Colmenares, J. Schmidt, M. F. Bekheet, B. R. Pauw, A. Gurlo, U. Simon, *Microporous Mesoporous Mater.* **2019**, *280*, 133.
11. D. Zhao, J. Feng, Q. Huo, N. Melosh, G. H. Fredrickson, B. F. Chmelka, G. D. Stucky, *Science* **1998**, *279*, 548.
12. L. M. Henning, J. T. Müller, G. J. Smales, B. R. Pauw, J. Schmidt, M. F. Bekheet, A. Gurlo, U. Simon, *Nanoscale Adv.* **2022**, *4*, 3892.
13. S.-H. Wu, C.-Y. Mou, H.-P. Lin, *Chem. Soc. Rev.* **2013**, *42*, 3862.
14. P. Schmidt-Winkel, W. W. Lukens, D. Zhao, P. Yang, B. F. Chmelka, G. D. Stucky, *J. Am. Chem. Soc.* **1999**, *121*, 254.

15. M. G. Colmenares, U. Simon, F. Schmidt, S. Dey, J. Schmidt, A. Thomas, A. Gurlo, *Microporous Mesoporous Mater.* **2018**, *267*, 142.
16. M. Shakeri, M. Shoda, *J. Mol. Catal. B Enzym.* **2010**, *62*, 277.
17. E. W. Ping, R. Wallace, J. Pierson, T. F. Fuller, C. W. Jones, *Microporous Mesoporous Mater.* **2010**, *132*, 174.
18. S. Nanaki, M. Tseklima, E. Christodoulou, K. Triantafyllidis, M. Kostoglou, D. N. Bikiaris, *Polymers* **2017**, *9*.
19. J. S. Lettow, Y. J. Han, P. Schmidt-Winkel, P. Yang, D. Zhao, G. D. Stucky J. Y. Ying, *Langmuir* **2000**, *16*, 8291.
20. J. Fan, C. Yu, L. Wang, B. Tu, D. Zhao, Y. Sakamoto, O. Terasaki, *J. Am. Chem. Soc.* **2001**, *123*, 12113.
21. W. Wang, W. Shan, X. Yue, H. Ru, *J. Mater. Chem.* **2012**, *22*, 3462.
22. D.-G. Choi, S.-M. Yang, *J. Colloid Interface Sci.* **2003**, *261*, 127.
23. B. Zhou, N. Qi, B. Wang, Z. Q. Chen, *Appl. Surf. Sci.* **2019**, *475*, 961.
24. W. Shan, W. Wang, H. Ru, *J. Non-Cryst. Solids.* **2015**, *425*, 183.
25. P. Schmidt-Winkel, W. W. Lukens, P. Yang, D. I. Margolese, J. S. Lettow, J. Y. Ying, G. D. Stucky, *Chem. Mater.* **2000**, *12*, 686.
26. Y. Han, S. S. Lee, J. Y. Ying, *Chem. Mater.* **2007**, *19*, 2292.
27. J. Kim, B. Song, G. Hwang, Y. Bang, Y. Yun, *J. Catal.* **2019**, *373*, 306.
28. C. J. Brinker, G. W. Scherer, *Sol-Gel Science: The Physics and Chemistry of Sol-Gel Processing*, Academic Press, Boston **2010**.
29. J. Kim, R. J. Desch, S. W. Thiel, V. V. Guliants, N. G. Pinto, *Microporous Mesoporous Mater.* **2012**, *149*, 60.
30. M. Kruk, L. Cao, *Langmuir* **2007**, *23*, 7247.
31. L. Huang, X. Yan, M. Kruk, *Langmuir* **2010**, *26*, 14871.
32. L. Huang, M. Kruk, *J. Colloid Interface Sci.* **2012**, *365*, 137.
33. S. Kerkhofs, T. Willhammar, H. van den Noortgate, C. E. A. Kirschhock, E. Breynaert, G. van Tendeloo, S. Bals, J. A. Martens, *Chem. Mater.* **2015**, *27*, 5161.
34. J. Jammaer, A. Aerts, J. D'Haen, J. W. Seo, J. A. Martens, *Scientific Bases for the Preparation of Heterogeneous Catalysts*, **2010**, pp. 681.
35. J. Rouquerol, P. Llewellyn, F. Rouquerol, *Stud. Surf. Sci. Catal.* **2007**, *160*, 49.
36. M. Thommes, K. Kaneko, A. V. Neimark, J. P. Olivier, F. Rodriguez-Reinoso, J. Rouquerol, K. S. Sing, *Pure Appl. Chem.* **2015**, *87*, 1051.
37. Quantachrome Instruments, autosorb iQ and ASiQwin Gas Sorption Operating Manual, **2015**.
38. B. Lippens, *J. Catal.* **1965**, *4*, 319.
39. G. J. Smales, B. R. Pauw, *J. Inst.* **2021**, *16*, P06034.
40. J. Filik, A. W. Ashton, P. C. Y. Chang, P. A. Chater, S. J. Day, M. Drakopoulos, M. W. Gerring, M. L. Hart, O. V. Magdysyuk, S. Michalik, A. Smith, C. C. Tang, N. J. Terrill, M. T. Wharmby, H. Wilhelm, *J. Appl. Crystallogr.* **2017**, *50*, 959.
41. B. R. Pauw, A. J. Smith, T. Snow, N. J. Terrill, A. F. Thünemann, *J. Appl. Crystallogr.* **2017**, *50*, 1800.
42. I. Breßler, J. Kohlbrecher, A. F. Thünemann, *J. Appl. Crystallogr.* **2015**, *48*, 1587.
43. M. G. Colmenares, U. Simon, M. Yildiz, S. Arndt, R. Schomaecker, A. Thomas, F. Rosowski, A. Gurlo, O. Goerke, *Catal. Commun.* **2016**, *85*, 75.
44. L. M. Henning, U. Simon, A. Gurlo, G. J. Smales, M. F. Bekheet, *RSC Adv.* **2019**, *9*, 36271.
45. S. A. Kube, K. Turke, R. Ellinghaus, D. Wallacher, M. Thommes, B. M. Smarsly, *Langmuir* **2020**, *36*, 11996.
46. DDBST GmbH, Saturated liquid density of p-xylene, http://ddbonline.ddbst.de/DIPPR105DensityCalculation/DIPPR105CalculationCGI.exe.
47. G. Karlström, *J. Phys. Chem.* **1985**, *89*, 4962.
48. P. Alexandridis, T. Alan Hatton, *Colloids Surf. A Physicochem. Eng.* **1995**, *96*, 1.
49. W. A. Pryor, R. E. Jentoft, *J. Chem. Eng. Data.* **1961**, *6*, 36.
50. B. Lefèvre, A. Galarneau, J. Iapichella, C. Petitto, F. Di Renzo, F. Fajula, Z. Bayram-Hahn, R. Skudas, K. Unger, *Chem. Mater.* **2005**, *17*, 601.
51. Y. Awoke, Y. Chebude, I. Díaz, *Molecules*, **2020**, *25*, 4909.
52. L. L. Hench, J. K. West, *Chem. Rev.* **1990**, *90*, 33.
53. J. W. M. Osterrieth, J. Rampersad, D. Madden, N. Rampal, L. Skoric, B. Connolly, M. D. Allendorf, V. Stavila, J. L. Snider, R. Ameloot, J. Marreiros, C. Ania, D. Azevedo, E. Vilarrasa-Garcia, B. F. Santos, X. H. Bu, Z. Chang, H. Bunzen, N. R. Champness, S. L. Griffin, B. Chen, R. B. Lin, B. Coasne, S. Cohen, J. C. Moreton, Y. J. Colón, L. Chen, R. Clowes, F. X. Coudert, Y Cui, et al., *Adv. Mater.* **2022**, *34*, e2201502.
54. M. Sridhar, G. K. Reddy, N. Hu, A. Motahari, D. W. Schaefer, S. W. Thiel, P. G. Smirniotis, *Microporous Mesoporous Mater.* **2014**, *190*, 215.
55. M. Thommes. *Nanoporous Materials: Science and Engineering* (Eds: M. Lu, G. X. Song Zhao), World Scientific Publishing Company, London **2004**, pp. 317.
56. S. Lowell, *Characterization of Porous Solids and Powders: Surface Area, Pore Size and Density*, Springer, **2004**.
57. P. I. Ravikovitch, A. V. Neimark, *J. Phys. Chem. B.* **2001**, *105*, 6817.
58. J. Sun, H. Zhang, D. Ma, Y. Chen, X. Bao, A. Klein-Hoffmann, N. Pfänder, D. S. Su, *Chem. Comm.* **2005**, 5343.
59. P. Holmqvist, P. Alexandridis, B. Lindman, *Macromolecules* **1997**, *30*, 6788.

SUPPORTING INFORMATION

Additional supporting information can be found online in the Supporting Information section at the end of this article.

How to cite this article: L. M. Henning, G. J. Smales, M. G. Colmenares, M. F. Bekheet, U. Simon, A. Gurlo, *Nano Select*. **2023**, 1. https://doi.org/10.1002/nano.202200223